

# Ion-Exchange Separators Suppressing Self-Discharge in Polymeric Supercapacitors

Kaiping Wang<sup>+</sup>, Lulu Yao,<sup>+</sup> Mehran Jahon, Jiaxi Liu, Matthew Gonzalez, Ping Liu, Vincent Leung, Xinyu Zhang, and Tse Nga Ng<sup>\*</sup>



Cite This: *ACS Energy Lett.* 2020, 5, 3276–3284



Read Online

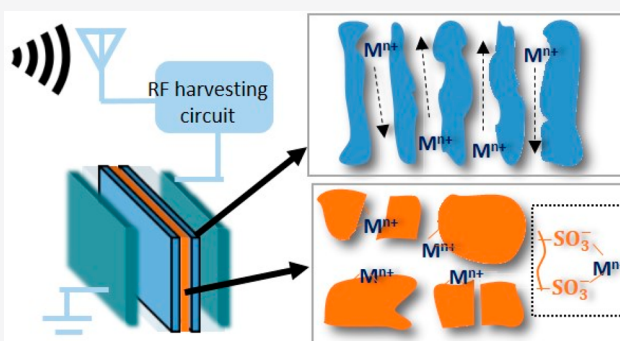
ACCESS |

Metrics & More

Article Recommendations

Supporting Information

**ABSTRACT:** Supercapacitors offer superior cycle life and high power densities, but as energy storage devices, they are limited by self-discharge processes manifested as large potential decay and leakage current, resulting in loss of stored energy and low charging efficiency. To minimize Faradaic side reactions, this Letter has incorporated a sulfonate ion-exchange resin in separators to trap impurities and thereby suppress self-discharge in supercapacitors with PEDOT as redox electrodes. The versatile separator design is generally applicable to organic and aqueous electrolytes and compatible with a pH range of 0–14, while maintaining the device capacitance and rate performance. Temperature-dependent characteristics were analyzed to identify that the reduction of impurity concentration and diffusion was key to improve potential retention. Compared to devices using commercially available separators, the device here exhibited a lower leakage current and better charging efficiency. It was demonstrated to work with radio frequency energy-harvesting circuits and showed the potential to serve as an energy reservoir for wireless electronic applications.



Energy storage devices are critical components that provide stable power for wireless electronics. While batteries are the dominant form of energy storage, supercapacitors offer superior cycle life and high power densities<sup>1–5</sup> and are being explored as alternatives to batteries, especially in settings that require only short-term energy storage, for example when integrated with an environmental energy harvester. However, the self-discharge processes<sup>6</sup> in supercapacitors have caused large potential decay and leakage current, resulting in loss of stored energy and low charging efficiency. Thus, it is crucial to understand and mitigate self-discharge phenomena in supercapacitors in order to take advantage of their potential as energy reservoirs with ultralong cycle life.<sup>7</sup>

When charged, a supercapacitor is in the high-energy state, and thermodynamically the device would discharge to a lower-energy state whenever there is a pathway. The self-discharge pathways are categorized into three types: charge redistribution, ohmic leakage, and Faradaic reactions.<sup>8</sup> Ohmic leakage and charge redistribution have been well-studied<sup>6,9</sup> and are now sufficiently suppressed to be a minor contributor to self-discharge processes, but the Faradaic reaction mechanism remains a challenging issue because of the difficulty in pinpointing side reactions, which could vary between electrode

materials, electrolyte ions, and unintentional impurities from different sources.

Recent research to minimize Faradaic self-discharge include modifying the electrode surface with a blocking layer,<sup>10</sup> and using liquid crystal additives in the electrolyte to impede the diffusion of redox species near the electrodes.<sup>11</sup> However, these approaches are not selective between electrolyte ions and redox impurities, and so the reduced self-discharge from limiting diffusion comes at a cost of lower rate performance and capacitance decrease. Alternatively, the use of novel electrode materials,<sup>12</sup> a proton exchange separator,<sup>13</sup> or a novel solid-state electrolyte<sup>14</sup> to confine cations have suppressed self-discharge, but these designs are specific for their material systems.

Building on the concept of trapping impurities to minimize Faradaic reactions, this Letter reports a versatile separator design that is generally applicable to aqueous and organic electrolytes while maintaining the device capacitance and rate

Received: August 17, 2020

Accepted: September 21, 2020

Published: September 29, 2020



ACS Publications

© 2020 American Chemical Society

3276

<https://dx.doi.org/10.1021/acsenergylett.0c01783>  
*ACS Energy Lett.* 2020, 5, 3276–3284

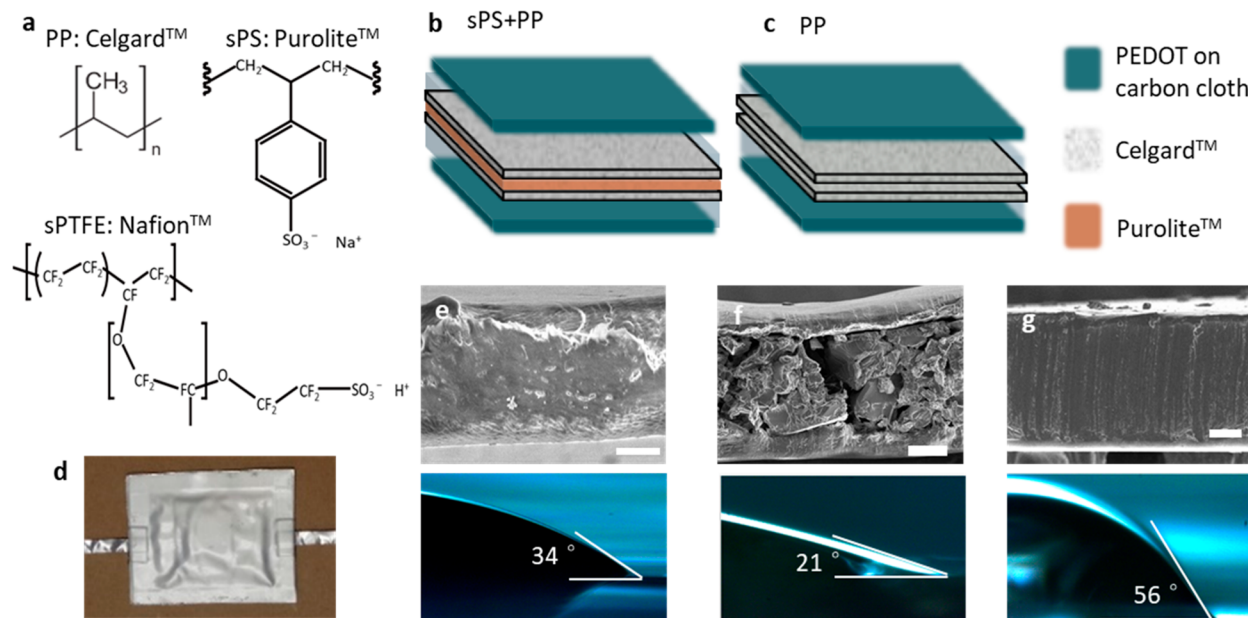


**Figure 1.** (a) Molecular structures of separator materials. Schematics of supercapacitor structures with separators consisting of (b) sPS+PP: Purolite sandwiched between two Celgard films and (c) PP: only two Celgard films. (d) Photograph of a supercapacitor pouch cell. For (e) PP, (f) sPS, and (g) sPTFE, the top row shows SEM images of the film cross sections. Scale bars: (d) 5  $\mu\text{m}$ , (e) 50  $\mu\text{m}$ , and (f) 50  $\mu\text{m}$ . The bottom row displays photographs of water contact angle measurements on the surface of the corresponding separator materials.

performance. In the modified separator, we incorporated a cation-exchange resin that is typically used for wastewater treatment to remove transition-metal ions. For our purpose, the resin suppressed the movement of redox impurities in the electrolyte by binding them to the polymer matrix and in exchange releasing an equivalent number of the resin cations back to electrolyte. In this way the impurities are collected in the separator without impeding electrolyte diffusion to keep up the device performance. The temperature dependence of the potential decline is monitored over 10 h and fitted to self-discharge models, to understand the self-discharge kinetics and compare thermal activation energies in devices with different separators.

To determine the potential of our supercapacitor as short-term storage devices, we proceeded to integrate our devices with a demonstration circuit that would harvest RF energy and store it in the supercapacitor. The implementation of energy-harvesting schemes is particularly critical for powering autonomous, wireless sensors and devices in Internet-of-Things (IoT) networks,<sup>15,16</sup> because it is not sustainable to manually replace empty primary batteries in billions of devices. The energy storage in our flexible supercapacitors will be relevant for applications such as wearable health monitors and environmental trackers. While there are many energy-harvesting approaches, including photovoltaics, mechanical generators, etc., in this work we focused on RF energy harvesting, considering that for all IoT applications, RF energy is already present in the associated wireless communications network.<sup>17</sup> We improved the leakage current and charging efficiency in devices to meet the requirements for wireless charging of supercapacitors.

The supercapacitors were fabricated using the redox-active polymer poly(3,4-ethylenedioxy-thiophene) (PEDOT) on carbon cloth current collectors. PEDOT is a mixed ionic and electronic conductor<sup>18–22</sup> with high stability<sup>23</sup> in supercapacitors. All the materials in our supercapacitor designs are

flexible and compatible with low-cost printing fabrication for IoT and wearable applications.<sup>16,24–27</sup>

Three types of separators were inserted between the electrodes to study how separator materials influence the supercapacitor performance and self-discharge characteristics. Figure 1a shows the molecular structures of separator materials as denoted by their commercial brand names. Celgard is a porous film made of polypropylene (PP), designed to block electron transport but allow ionic diffusion. Nafion is a fluoropolymer backbone with sulfonate groups (sPTFE) that allow high proton conductivity. PP and sPTFE are routinely used as separators in energy storage devices including batteries, supercapacitors, and fuel cells. Purolite is a polystyrene resin with sulfonate end groups (sPS), which show the highest cation adsorption capacity among ion-exchange functional groups (capacity of adsorbing 12 mg of transition-metal ions per gram of sPS resin),<sup>28–30</sup> and is mainly used to separate heavy metal ions in water treatment. Here we repurposed it for retarding redox impurities in the separator to minimize unwanted reactions in supercapacitors. As the sPS resin cannot form a free-standing film, it was made into a layer sandwiched between two PP films to form a separator stack (sPS+PP) as shown in Figure 1b. For comparison, the other separator stacks in this work were a single sPTFE film (183  $\mu\text{m}$  in thickness) or two PP films (each 25  $\mu\text{m}$  in thickness) without the sPS layer (Figure 1c). We used a single sPTFE film to keep the separator thickness comparable to the sPS+PP stack, to minimize the equivalent series resistance of the device. Supercapacitors with different separators were made into pouch cells (Figure 1d).

The water contact angle measurements in Figure 1e–g shows the hydrophobicity of the separator materials, with sPTFE ( $56^\circ$ ) > PP ( $34^\circ$ ) > sPS ( $21^\circ$ ). The molecular structure of sPS has a high volume ratio of hydrophilic functional groups to the polymer backbone, thus increasing hydrophilicity and contact with aqueous electrolytes. The scanning electron microscopy (SEM) image in Figure 1f displays that the sPS

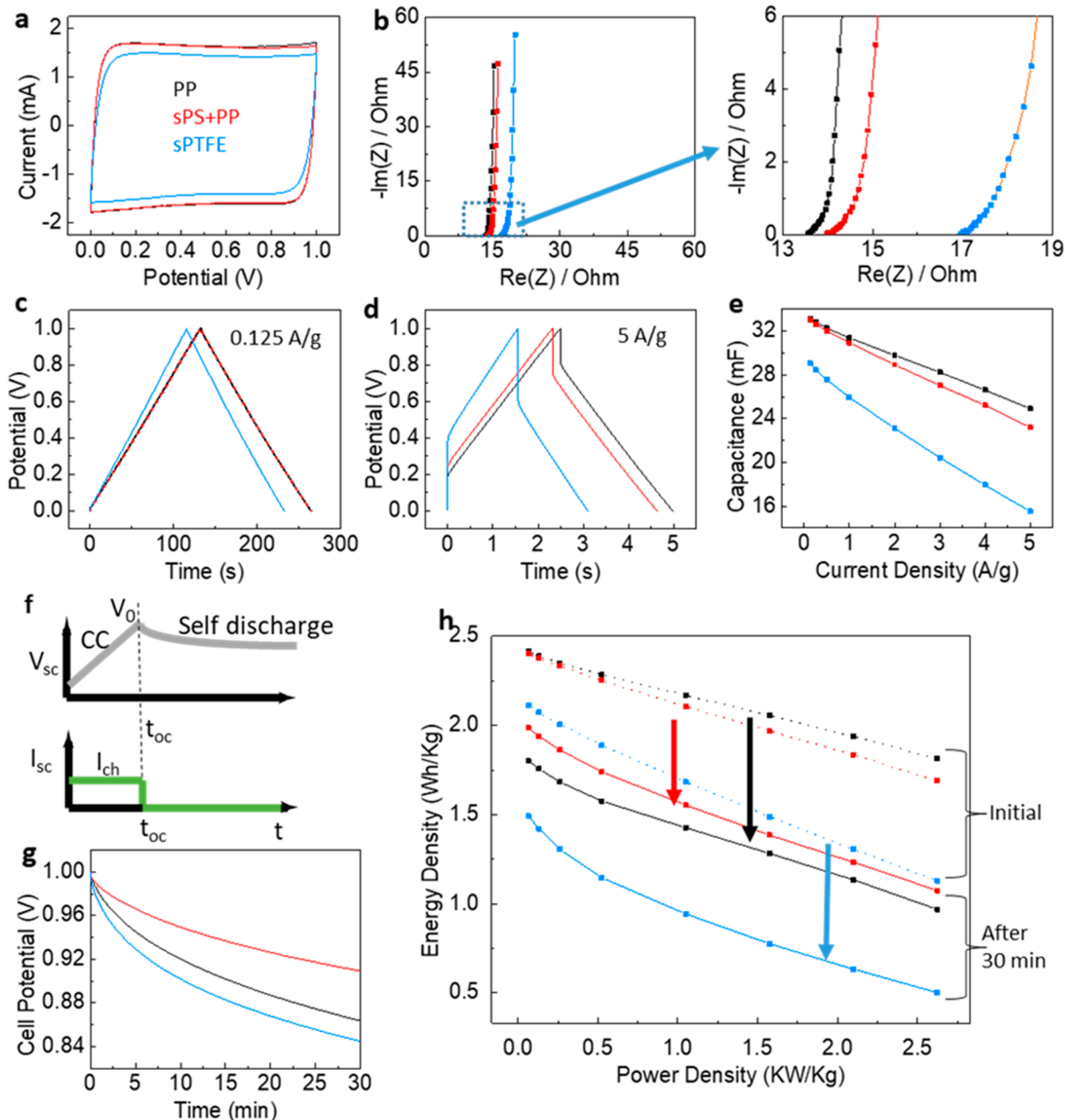


**Figure 2.** Performance comparison of supercapacitors with different separators: PP (black), sPS+PP (red), and (f) sPTFE (blue). The color legend applies to all subplots. (a) Current versus voltage, at a scan rate of 50 mV/s. (b) Imaginary versus real impedance. The right plot zooms in on the high-frequency region. (c) Galvanostatic charge–discharge characteristics with constant current at (c) 0.125 A/g and (d) 5 A/g. (e) Capacitance versus charging current density. (f) Schematic of the self-discharge measurement, in which a constant current (CC) is applied to reach the end potential  $V_0$  and subsequently the change in voltage due to self-discharge is monitored starting at time  $t_{oc}$ . (g) Self-discharge characteristics versus time, after charging at a constant current density of 0.5 A/g to a terminal potential of 1 V. The electrolyte was 1 M KCl in deionized water. (h) Energy densities versus power densities, before and after 30 min of self-discharge.

layer was roughly packed. For the separator stack in Figure 1b, the dense columnar structures in PP films (Supplemental Figure S1) encased the sPS layer to form an electrical insulator with pathways for ionic diffusion. The next two sections compare the supercapacitor characteristics as a function of time and temperature, to determine the self-discharge mechanisms and kinetics in these devices with different separators.

**Characterization of Supercapacitor Performance.** Given that the electrodes and electrolyte were the same across the devices, the differences in cell performance are attributed to the

separators. The cyclic voltammograms in Figure 2a indicate similar current–voltage characteristics in supercapacitors with PP and sPS+PP separators, and these devices showed higher current than the one with sPTFE. In Figure 2b, the equivalent series resistance (ESR) was worst in the device using sPTFE, followed by sPS+PP and then PP, although the ESR difference in devices with or without sPS was only 0.5 Ω. The sPS layer did not affect the device performance at low charge–discharge rate. For instance, in Figure 2c at a current density of 0.125 A/g, the galvanostatic charge–discharge (GCD) curves were found to be the same for the supercapacitors with PP only and

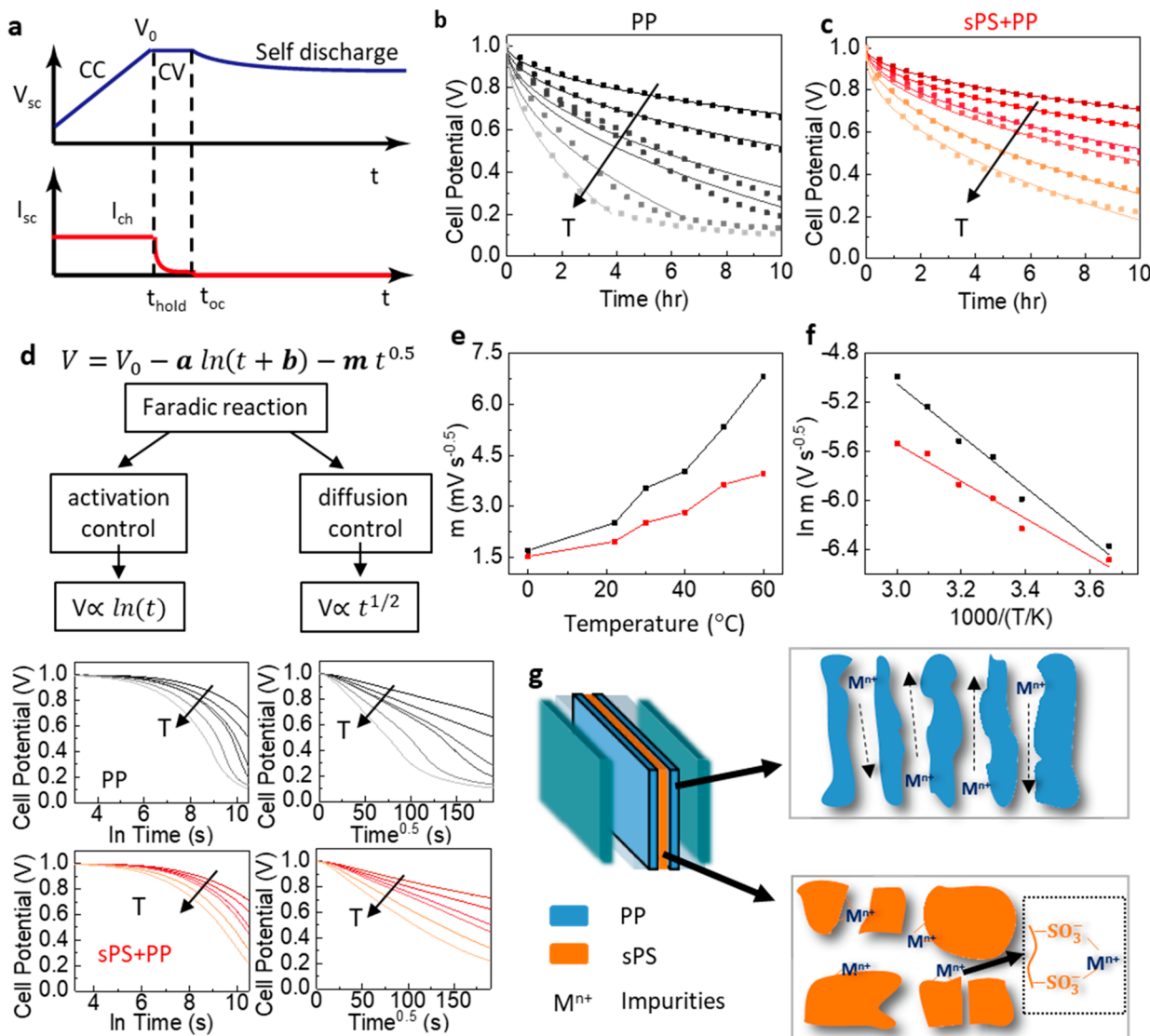


**Figure 3. Comparison of self-discharge mechanisms in supercapacitors using PP (black) and sPS+PP (red) separators. The color legend applies to all subplots. (a)** Schematic of the self-discharge measurement with a constant potential hold before self-discharge is monitored starting at time  $t_{oc}$ . **(b and c)** Self-discharge characteristics at different temperatures ( $T = 0, 22, 30, 40, 50, 60$  °C). The solid lines represent fitting results to eq 1. **(d)** Relationship of potential versus time, as a function of  $\ln t$  or  $t^{0.5}$ . The fit values of  $m$  versus temperature, shown in **(e)** a linear scale and **(f)** a natural logarithmic scale for determining thermal activation energies. **(g)** Schematic illustrating the capture of cationic impurities by sulfonate functional groups.

with sPS+PP. As the charge–discharge current density was increased to 5 A/g in Figure 2d, larger IR drops were observed and correlated to the ESR trend. GCD curves in Supplemental Figure S2 were used to calculate the capacitance in Figure 2e by the relation  $C = I/(dV/dt)$ , where  $I$  is the discharge current and  $dV/dt$  is the voltage change measured per recording time interval. The device with sPS+PP showed as much as 1.5 times higher capacitance than the one with SPTFE. When compared to the control device with PP only, the device with sPS+PP demonstrated similar capacitance, with at most 10% decrease as the charge–discharge current density was raised to 0.5 A/g. Thus, the rate performance of supercapacitors was not significantly impacted by incorporating a sPS layer.

In typical use cases, supercapacitors are charged by a current input, and when the desired voltage is reached, the charging current is switched off. Then the device is placed in the open-circuit condition to hold its energy, to be discharged only as

needed. However, self-discharge processes may occur within the cell, leading to a reduction in the device potential. From the time at which charging was stopped (denoted as  $t_{oc}$  in Figure 2f), the potential of the supercapacitor was periodically measured, and the cell voltage was shown to decay over time in Figure 2g. The potential decay increased as the charging current density was raised from 0.125 to 0.5 A/g (Supplemental Figure S3). The potential retention was the best in the device with sPS+PP, with its voltage maintained at 91% of the initial value after 30 min; the voltage in devices with PP and sPTFE decreased to 86% and 84%, respectively.

The potential decay due to self-discharge affects the device energy densities. Figure 2h reveals that initially the supercapacitor with the PP separator was the most energy dense, owing to its ESR being the lowest among the devices. But after 30 min of holding in open circuit, the retained energy of the device with sPS+PP surpassed the one with PP only. The

additional sPS layer was essential in suppressing energy dissipation due to self-discharge.

The energy densities reported in Figure 2h are comparable to prior works<sup>18,31</sup> using PEDOT as Faradaic electrodes (Supplemental Figure S4). The notable point here is that the voltage decay was greatly reduced by modifying the separator. Because the device with sPTFE showed the lowest energy density and rate performance, and its voltage also degraded the most during the open-circuit interval, sPTFE was not included in further analysis.

**Analysis of Self-Discharge Mechanisms.** To understand how the sPS layer improved voltage retention, we recorded the change in cell voltage over time at various temperatures and tested the data against self-discharge models.<sup>8,32</sup> Here the charging method included a hold at the terminal voltage, as seen in Figure 3a. This constant voltage (CV) segment was introduced to eliminate self-discharge due to charge redistribution. Charge redistribution occurs when there is a charge gradient from the surface to the bulk of the electrode materials,<sup>33</sup> but by applying a 1 h CV hold, charge inhomogeneity in electrodes would have sufficient time to equilibrate and become negligible. In this way we excluded effects of charge redistribution and focused on self-discharge mechanisms due to Faradaic reactions.

Figure 3b,c displays the change in voltage over 10 h in devices with PP and sPS+PP separators, after they were charged to 1 V and held at this terminal voltage for 1 h. The data are fitted to the equation below, which was derived in ref 8 to relate the potential change to activation-control or diffusion-control Faradaic reactions (Figure 3d):

$$V(t) = V_0 - a \ln(t + b) - m\sqrt{t} \quad (1)$$

where  $t$  is time and  $V_0$  is the initial voltage at the start of the open-circuit condition; the term  $a \ln(t + b)$  is due to over-potential activation of decomposition reactions that discharge electrodes, and the term  $m\sqrt{t}$  is related to diffusion-limited side reactions caused by a low concentration of redox impurities.<sup>8</sup> The device operating at elevated temperatures in Figure 3b showed fast self-discharge and reached nearly 0 V at the end of the self-discharge process. When the potential is near zero, eq 1 is no longer applicable. Nonetheless, most of the self-discharge characteristics are fitted well by eq 1. On the basis of eq 1, if the origin of self-discharge is dominantly activation-controlled reactions, there would a linear relationship between  $V$  and  $\ln t$ . On the other hand, if the self-discharge mechanism is diffusion-controlled, the plot of  $V$  versus  $\sqrt{t}$  would be linear.

From Figure 3d, for both PP and sPS+PP separators, the device characteristics follow a linear relationship when plotted as  $V$  versus  $\sqrt{t}$ , indicating that diffusion-limited reactions were the determining factor in self-discharge processes. In fact, in simplifying eq 1 and eliminating the activation term, the values of  $m$  obtained from fitting data to  $V(t) = V_0 - m\sqrt{t}$  are essentially the same as fitting to the full eq 1 (fit values listed in Supplemental Tables S1 and S2); results from either fit approach differ by less than 1%.

In Figure 3e, the fit values of  $m$  show temperature dependence, reflecting the trend that the potential decay was larger as temperature was increased from 0 to 60 °C. In the diffusion-control model, the variable  $m$  is expressed in physical parameters<sup>6,8,34</sup> as  $m = 2zFAc_r\sqrt{D}/(C\sqrt{\pi})$ , where  $z$  is the stoichiometric number of electrons in the reaction,  $F$  Faraday's

constant,  $A$  electrode area,  $c_r$  the initial concentration of reacting species,  $D$  the diffusion coefficient, and  $C$  the device capacitance. The parameters  $z$ ,  $F$ ,  $A$ , and  $C$  are the same between the supercapacitors, and thus, any difference in  $m$  is due to concentration  $c_r$  or diffusion rate  $D$  of impurities. Across the temperature range, the  $m$  value was smaller in the supercapacitor with sPS than the one without it, showing that the sPS layer minimized impurity concentration and/or diffusion better than conventional PP separators.

In Figure 3f, the temperature dependence of  $m$  was further analyzed by using the Arrhenius equation:  $\ln(m) = \ln(m_0) - E_a/RT$ , where  $E_a$  is the thermal activation energy,  $T$  the temperature,  $R$  the ideal gas constant, and  $m_0$  the pre-exponential factor. The extracted values are  $E_a = 17.5 \text{ kJ mol}^{-1}$  and  $m_0 = 3.58 \text{ mV s}^{-0.5}$  for the device with PP and  $E_a = 12.6 \text{ kJ mol}^{-1}$  and  $m_0 = 0.34 \text{ mV s}^{-0.5}$  for the other with sPS+PP. The  $m_0$  factor is temperature-independent and proportional to the impurity concentration, with the lower value indicating the sPS+PP-based system showed a low impurity concentration. Meanwhile, because diffusion is thermally activated, it is influenced by  $E_a$ . A low  $E_a$  value implied that the change in diffusion rate with temperature is small. As such, the potential decay in the supercapacitors using sPS+PP separator is less severe with rising temperature, compared to the device with only PP.

Thus, the above analyses suggest that the sulfonate groups in sPS can suppress self-discharge through two mechanisms, by decreasing the concentration of redox impurities through ion-exchange adsorption and by slowing down the diffusion of impurities. The impurities that cause self-discharge reactions are likely transition-metal ions, for example  $\text{Fe}^{2+}/\text{Fe}^{3+}$  found in carbon electrodes.<sup>35</sup> Figure 3g illustrates the different interactions between transition-metal ions  $M^{n+}$  and the separator material. Whereas PP films contain porous, columnar conduits for all ions to pass through, sPS is a strong cationic exchange resin and preferentially retain impurity ions  $M^{n+}$  over electrolyte cations ( $\text{K}^+$  or  $\text{H}^+$ ), as the impurities are in high oxidation states and strongly bound to the sulfonate groups on the separator. We have intentionally added  $\text{FeCl}_3$  as impurities into the electrolyte, and the changes in the self-discharge rate as a function of  $\text{Fe}^{3+}$  concentrations are shown in Supplemental Figure S5.

In addition to the aqueous KCl electrolyte with neutral pH 7, a highly acidic (0.5 M  $\text{H}_2\text{SO}_4$ , pH 0) or alkaline (1 M KOH, pH 14) electrolyte was used for the supercapacitors to study the effect of pH on potential decay. The decay was the most severe with the alkaline electrolyte, then the acidic one, and least with the neutral electrolyte (Supplemental Figure S6).<sup>36</sup> The PEDOT electrodes are known to be more stable in acidic than alkaline environments. The rate of self-discharge in acidic electrolytes was slightly worse than in neutral, because of a higher concentration of  $\text{H}^+$  that competes with the exchange of impurity ions, resulting in less effective adsorption of the impurities. Nonetheless, regardless of pH, the sPS+PP separator consistently reduced the cell potential decay better than PP alone, implying that the ion-exchange function is maintained over the entire pH range.

Besides aqueous electrolytes, organic electrolyte (0.5 M tetraethylammonium tetrafluoroborate TEABF<sub>4</sub> in propylene carbonate PC) was also used in the supercapacitors, and again the sPS+PP separator was beneficial to suppress potential decay in these cells, with only 15% loss in potential after an open-circuit period of 10 h, compared to the 25% loss in the

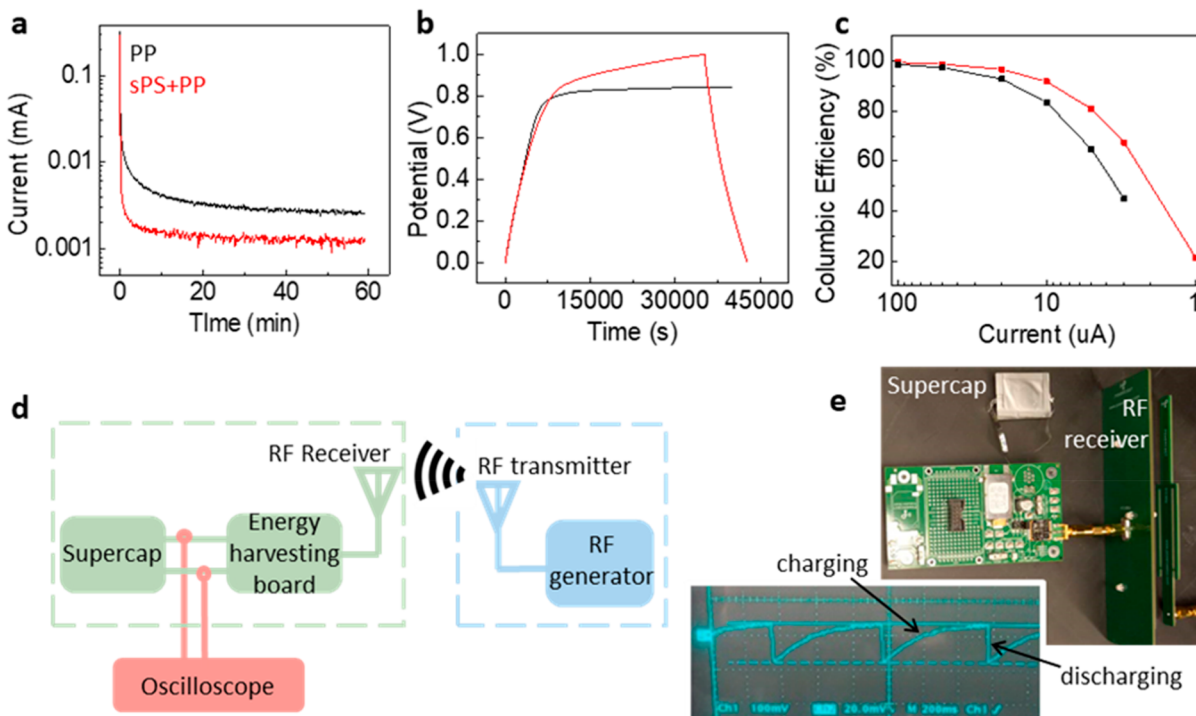


**Figure 4.** (a) Leakage current in supercapacitors with different separators in 1 M KCl electrolyte. (b) Galvanostatic charge–discharge characteristics at a constant current input of 1  $\mu$ A (current density = 0.5 mA/g). The device with PP was not discharged because it did not reach the terminal voltage of 1 V. (c) Coulombic efficiency for supercapacitors at various current levels. (d) Schematic and (e) photograph of the RF energy-harvesting circuit connected to a supercapacitor pouch cell. The photograph of the oscilloscope screen shows voltage changes with charging and discharging of the supercapacitor. For this near-field transmission setup, the charging power was 178  $\mu$ W.

device with only PP (Supplemental Figure S7). Overall, the sPS+PP separator shows its wide applicability to reduce impurity side reactions in various aqueous and organic electrolyte systems.

*Requirement to Minimize Leakage Current in Wireless RF Energy-Harvesting Applications.* As we have clarified the role of sPS in mitigating self-discharge in our supercapacitors, we proceeded to integrate our devices with a demonstration circuit that would harvest RF energy and store it in the supercapacitor, which then can serve as the power source for numerous electronic applications. Because environmental energy harvesting is intermittent by its nature, the storage supercapacitor in the energy-harvesting circuit serves an important role as a continuously available energy reservoir. While the intricacies of power management, such as the duty cycle, peak and quiescent power, etc., in RF energy-harvesting circuits are discussed in prior work such as refs 17 and 37, here we are mainly concerned about the key issue of leakage current<sup>38,39</sup> which must be mitigated in order to use supercapacitors in energy-harvesting circuits.

Leakage current of the storage devices must be less than the input current, otherwise charge will be draining faster than coming in and the device will never reach the desired terminal voltage. While near-field RF density is permitted<sup>17</sup> to be up to 1 mW/cm<sup>2</sup>, environmental RF radiation power typically varies between 1 and 200  $\mu$ W/cm<sup>2</sup>, and so we assume that to charge a supercapacitor to reach 1 V, the charging current will be on the order of microamperes. The leakage current of supercapacitors is often in the microampere range, originating from charge redistribution and the same side reactions causing self-discharge and potential decay. We recorded the leakage currents of our supercapacitors with different separators by

monitoring the current flow needed to maintain the cell at a constant voltage (the segment between  $t_{\text{hold}}$  and  $t_{\text{oc}}$  in Figure 3a). The leakage current is  $\sim 3 \mu$ A in the device with PP and  $\sim 1 \mu$ A in the one with sPS+PP, for the condition of 1 V bias in Figure 4a.

We note that leakage is dependent on the cell potential;<sup>33</sup> that is, if the potential decreases, the driving force for spontaneous discharge reactions also decreases, resulting in a smaller leakage current. This voltage dependence leads to the characteristics in Figure 4b, where initially the devices were able to accumulate the input charge and showed increasing cell voltage when the leakage is small at low potential. However, as the potential reached above 0.7 V, the corresponding leakage current increased, making it more difficult to accrue incoming charge; hence, the rise in voltage slowed down. The supercapacitor with the PP separator was not able to get to the terminal voltage of 1 V when the input current was at 1  $\mu$ A. Meanwhile, the device with sPS+PP reached the target of 1 V, indicating that its leakage current was  $\leq 1 \mu$ A for the whole potential range.

Figure 4c shows the Coulombic efficiencies of our devices as a function of the input current level, to compare the ratio of the output charge to the input charge in a charge–discharge cycle. Coulombic efficiencies are calculated from GCD curves (Supplemental Figure S8) and typically used to evaluate the extent of side reactions, and we can also interpret it in the context of leakage problems. For charging current above 20  $\mu$ A (equivalent to a current density of 10 mA/g), the efficiency is near 100% for the device with sPS+PP separator, meaning that there is no loss in storage and all the input energy is completely returned during output delivery. With lower charging current, the difference between charging time and discharging time

becomes larger (Figure 4b), and the Coulombic efficiency gradually reduced, down to 22% when the current was at 1  $\mu$ A. The supercapacitors can become inefficient at charge storage and delivery in low-power systems. Nonetheless, on an encouraging note, Figure 4c points out that the devices are well suited for charging current above 20  $\mu$ A, which is easily met by the input from energy-harvesting photovoltaic cells. Moreover, the sPS+PP separator enables reduction of the device leakage current, superior to that of standard commercial supercapacitors (comparisons in *Supplemental Figure S9*); it helps the retention of energy density when the cell is at open-circuit state, as well as increases the efficiency of the charging–discharging process.

To test if our supercapacitor with the sPS+PP separator can work in RF energy-harvesting applications, we connected the pouch cell to the commercially available circuit board Powercast P2110, which converted 915 MHz RF signals to supply direct current to the storage device (Figure 4d). This wireless energy harvester worked in near field, with working distance up to 6 cm. The voltage of the supercapacitor was monitored on an oscilloscope as the circuit charged and discharged. The voltage rails for this demonstration were set at 1.0 and 1.25 V. That is, when the supercapacitor was at 1.0 V, the harvester circuit initiated the charging process to bring up the supercapacitor voltage to 1.25 V. Upon reaching 1.0 V, the harvester circuit was programmed to discharge the supercapacitor, which supplied current to light up a light-emitting diode. When the voltage dropped back to 1.0 V, charging restarted, and the cycles of charging and discharging are repeated. Such voltage cycles are shown in the photograph of Figure 4e, and the charging time was 6 s at an input power of 178  $\mu$ W. This demonstration has achieved wireless charging of our low-leakage supercapacitor and revealed the potential of our device in RF energy-harvesting applications.

In conclusion, this work has successfully incorporated a sulfonate ion-exchange resin in separators to trap impurities and thereby suppress self-discharge reactions in supercapacitors with PEDOT as redox electrodes. The cation exchange mechanism in the sPS-modified separator was universally effective with organic and aqueous electrolytes and in the pH range from 0 to 14. After 10 h in open circuit, the device with a sPS+PP separator was shown to retain 70% of its terminal voltage in the aqueous electrolyte (KCl in DI water) and 85% in the organic one (TEABF<sub>4</sub> in PC) at room temperature. The supercapacitors with sPS+PP separators maintained their potential better than the ones with conventional sPTFE or PP films, without sacrificing the rate performance or specific capacitance.

The temperature-dependent characteristics of potential decay were found to match the diffusion-limited self-discharge model, indicating that reduction of redox impurity concentration and diffusion was key to improve potential retention. For the device with a sPS+PP separator, the leakage current was sufficiently low, and the supercapacitor was demonstrated to work with RF energy-harvesting circuits. The Coulombic efficiency of our pouch cell was improved by the sPS+PP separator, to serve as an energy reservoir in systems with low charging current. Lastly, beyond supercapacitors, this work may be applicable to separator designs in other storage devices such as batteries and fuel cells to mitigate deleterious effects from diffusion of transition-metal contaminants between electrodes.

## ■ EXPERIMENTAL PROCEDURES

**Electrode Fabrication.** PEDOT electrodes were prepared by drop casting an aqueous solution of poly(3,4-ethylenedioxithiophene) polystyrenesulfonate (PEDOT:PSS, Clevios P1000) on a (0.5 cm)<sup>2</sup> square carbon cloth electrode (AvCarb MGL190). After drying at 120 °C for 30 min, the electrodes were immersed in concentrated H<sub>2</sub>SO<sub>4</sub> (wt. 98%) for 1 h under vacuum to etch away the PSS component and leave behind PEDOT with enhanced conductivity.<sup>40</sup> Then the electrodes were washed with DI water 3 times to remove residual acid, followed by drying at 120 °C for 30 min.

**Separator Fabrication.** Celgard 3501 (Porosity 55%, pore size 65 nm) and Nafion 117 (Chemours) were used as purchased and were 25 and 183  $\mu$ m in thickness, respectively. The films were cut into circular pieces with 0.5 cm diameter by using a hole puncher. To prepare the separator with Purolite CE100, a solution of the Purolite resin, sodium carboxymethyl cellulose (CMC) (Sigma, molecular weight: ~9000), and deionized (DI) water was put together at a weight ratio of 1.8:0.2:8, and the mixture was then grinded into a slurry in an agate mortar. A 100  $\mu$ L aliquot (~18 mg Purolite) of this slurry was drop-cast on a 1.3 cm<sup>2</sup> piece of Celgard film. Then another piece of Celgard film was placed on top and dried at 60 °C for 10 min. The CMC acted as a binder to glue the two films together to form a separator with a total thickness of ~200  $\mu$ m. In the future, the sPS layer can be tuned to a lower thickness if desired, by reducing the Purolite particle size and amount in the slurry.

**Pouch Cell Fabrication.** The supercapacitors consisted of two PEDOT electrodes, using 200 and 400  $\mu$ L of PEDOT:PSS for cathode and anode, respectively. The estimated mass of active materials is 0.63 and 1.26 mg for cathode and anode, respectively. The mass ratio of 2 is used to provide excess anode materials. Then Al foils (Hunan Hong Xiang New Energy Technology CO. Ltd.) with larger size than electrodes were welded with electrode tabs by an ultrasonic spot-welder (MTI MSK-800W) to form current collectors for carbon cloth electrodes. This step was done because carbon cloth cannot be directly welded to an electrode tab. Then the stack was placed in an aluminum-coated bag, and 200  $\mu$ L of 0.5 M TEABF<sub>4</sub> in PC was added as electrolyte. Finally, the aluminum plastic bag was sealed by a vacuum presealing machine (MTI MSK-115A-S), and the excess electrolyte was also removed.

**Materials Characterization.** Scanning electron microscopy measurements were carried out on an FEI scanning electron microscope at 5 kV for morphology observation. Water contact angle measurement was taken with a camera pointing orthogonally to the sample surface. A side view of a DI water droplet on top of the sample surface was captured by the camera. The samples with areas of ~1.5 cm × 1.5 cm were fixed on glass slides with tape, and DI water droplets were delivered onto the sample surface by a syringe. The ion capture capacity of sPS was studied by adding different concentrations of FeCl<sub>3</sub> (Fisher Science, Reagent grade, S25317A) as impurities into the device electrolyte.

**Electrochemical Characterization.** Electrochemical measurements were carried out via a BioLogic SP-200 potentiostat on samples in the two-electrode configuration, with the electrodes submerged in different electrolytes in a Swagelock cell or a pouch cell. The aqueous electrolytes were 1 M KCl, 0.5 M H<sub>2</sub>SO<sub>4</sub>, and 1 M KOH in DI water. The organic electrolyte was 0.5 M TEABF<sub>4</sub> in PC solvent, and measurements using the

organic electrolyte were carried out inside a nitrogen glovebox. The anode and cathode were made in the same way as described above in the pouch cell procedure. Cyclic voltammetry was scanned between 0 and 1 V at 50 mV/s. Electrochemical impedance spectroscopy was performed at the open-circuit voltage with an amplitude of 10 mV and frequencies ranging from 200 kHz to 10 mHz. Galvanostatic charge–discharge cycles were conducted at 0.125, 0.25, 0.5, 1, 2.5, and 5 A/g between 0 and 1 V. For self-discharge measurements, if a potential change higher than 5 mV was observed, the corresponding time was recorded. Thus, during the initial several minutes of a self-discharge test, data points were recorded for every 5 mV drop. Later, if the 5 mV drop took longer than 60 s, the recording method was switched to taking one data point every 60 s.

The energy density of a supercapacitor is calculated by the equation  $E = CV^2/2$ , where  $C$  is the specific capacitance and  $V$  is the retained voltage. The power density depends on how quickly the stored energy can be released and is determined according to the equation  $P = E/\Delta t$ , in which  $\Delta t$  is the discharge time.

**RF Energy-Harvesting Circuit.** The RF energy-harvesting circuit was taken from the P2110 Evaluation Board (Powercast). This board converted RF energy into DC power, and we disconnected the on-board storage capacitor and replaced it with our own pouch cell. The RF transmitting and receiving were done with a 915 MHz PCB dipole antenna and a 915 MHz PCB patch antenna, respectively. The transmitting signal was generated by a RF signal generator (Fluke 6062A), and the voltage on the pouch cell was monitored with an oscilloscope (Tektronix TDS 40A).

## ■ ASSOCIATED CONTENT

### SI Supporting Information

The Supporting Information is available free of charge at <https://pubs.acs.org/doi/10.1021/acsenergylett.0c01783>.

(1) Scanning electron microscopy images; (2) GCD curves and SDC characteristics of supercapacitors based on PP, sPS, and sPS+PP; (3) SDC characteristics after adding different concentrations of transition-metal ions as impurities into the electrolyte; (4) SDC characteristics of sPS in different electrolytes; (5) GCD curves at current density from 1 uA to 100 uA; (6) leakage current comparison with commercial supercapacitors; (7) equipment and circuits for RF charging process; (8) fitting results of the SDC process at different temperatures ([PDF](#))

## ■ AUTHOR INFORMATION

### Corresponding Author

Tse Nga Ng – Materials Science Engineering Program and Department of Electrical and Computer Engineering, University of California San Diego, La Jolla, California 92093, United States;  orcid.org/0000-0001-6967-559X; Email: [tng046@ucsd.edu](mailto:tng046@ucsd.edu)

### Authors

Kaiping Wang – Materials Science Engineering Program, University of California San Diego, La Jolla, California 92093, United States

Lulu Yao – Materials Science Engineering Program, University of California San Diego, La Jolla, California 92093, United States

Mehran Jahon – Department of Electrical and Computer Engineering, University of California San Diego, La Jolla, California 92093, United States

Jiaxi Liu – Department of Electrical and Computer Engineering, University of California San Diego, La Jolla, California 92093, United States

Matthew Gonzalez – Materials Science Engineering Program, University of California San Diego, La Jolla, California 92093, United States

Ping Liu – Materials Science Engineering Program, University of California San Diego, La Jolla, California 92093, United States

Vincent Leung – Department of Electrical and Computer Engineering, University of California San Diego, La Jolla, California 92093, United States

Xinyu Zhang – Department of Electrical and Computer Engineering, University of California San Diego, La Jolla, California 92093, United States

Complete contact information is available at:  
<https://pubs.acs.org/10.1021/acsenergylett.0c01783>

### Author Contributions

<sup>†</sup>K.W. and L.Y. contributed equally to this work.

### Notes

The authors declare no competing financial interest.

## ■ ACKNOWLEDGMENTS

The authors K.W., L.Y., V.L., X.Z., and T.N.N. are grateful for the support from National Science Foundation CNS-1901048. Part of the work was performed at the San Diego Nanotechnology Infrastructure of UCSD, which is supported by NSF ECCS-1542148.

## ■ REFERENCES

- Kim, B. C.; Hong, J. Y.; Wallace, G. G.; Park, H. S. Recent Progress in Flexible Electrochemical Capacitors: Electrode Materials, Device Configuration, and Functions. *Adv. Energy Mater.* **2015**, *5* (22), 1500959.
- Wang, F.; Wu, X.; Yuan, X.; Liu, Z.; Zhang, Y.; Fu, L.; Zhu, Y.; Zhou, Q.; Wu, Y.; Huang, W. Latest Advances in Supercapacitors: From New Electrode Materials to Novel Device Designs. *Chem. Soc. Rev.* **2017**, *46* (22), 6816–6854.
- Salanne, M.; Rotenberg, B.; Naoi, K.; Kaneko, K.; Taberna, P.-L.; Grey, C. P.; Dunn, B.; Simon, P. Efficient Storage Mechanisms for Building Better Supercapacitors. *Nat. Energy* **2016**, *1* (6), 16070.
- Simon, P.; Gogotsi, Y.; Dunn, B. Where Do Batteries End and Supercapacitors Begin? *Science* **2014**, *343* (6176), 1210–1211.
- Wang, Y.; Su, S.; Cai, L.; Qiu, B.; Wang, N.; Xiong, J.; Yang, C.; Tao, X.; Chai, Y. Monolithic Integration of All-in-One Supercapacitor for 3D Electronics. *Adv. Energy Mater.* **2019**, *9* (15), 1900037.
- Andreas, H. A. Self-Discharge in Electrochemical Capacitors: A Perspective Article. *J. Electrochem. Soc.* **2015**, *162* (5), A5047–A5053.
- Kamboj, N.; Purkait, T.; Das, M.; Sarkar, S.; Hazra, K. S.; Dey, R. S. Ultralong Cycle Life and Outstanding Capacitive Performance of a 10.8 v Metal Free Micro-Supercapacitor with Highly Conducting and Robust Laser-Irradiated Graphene for an Integrated Storage Device. *Energy Environ. Sci.* **2019**, *12* (8), 2507–2517.
- Conway, B. E.; Pell, W. G.; Liu, T.-C. Diagnostic Analyses for Mechanisms of Self-Discharge of Electrochemical Capacitors and Batteries. *J. Power Sources* **1997**, *65* (1), 53–59.
- Zhang, Q.; Rong, J.; Ma, D.; Wei, B. The Governing Self-Discharge Processes in Activated Carbon Fabric-Based Supercapacitors with Different Organic Electrolytes. *Energy Environ. Sci.* **2011**, *4* (6), 2152–2159.

- (10) Tevi, T.; Yaghoubi, H.; Wang, J.; Takshi, A. Application of Poly (p-Phenylene Oxide) as Blocking Layer to Reduce Self-Discharge in Supercapacitors. *J. Power Sources* **2013**, *241*, 589–596.
- (11) Xia, M.; Nie, J.; Zhang, Z.; Lu, X.; Wang, Z. L. Suppressing Self-Discharge of Supercapacitors via Electrorheological Effect of Liquid Crystals. *Nano Energy* **2018**, *47*, 43–50.
- (12) Wang, Z.; Xu, Z.; Huang, H.; Chu, X.; Xie, Y.; Xiong, D.; Yan, C.; Zhao, H.; Zhang, H.; Yang, W. Unraveling and Regulating Self-Discharge Behavior of  $Ti_3C_2T_x$  MXene-Based Supercapacitors. *ACS Nano* **2020**, *14* (4), 4916–4924.
- (13) Chen, L.; Bai, H.; Huang, Z.; Li, L. Mechanism Investigation and Suppression of Self-Discharge in Active Electrolyte Enhanced Supercapacitors. *Energy Environ. Sci.* **2014**, *7* (5), 1750–1759.
- (14) Wang, Z.; Chu, X.; Xu, Z.; Su, H.; Yan, C.; Liu, F.; Gu, B.; Huang, H.; Xiong, D.; Zhang, H.; et al. Extremely Low Self-Discharge Solid-State Supercapacitors via the Confinement Effect of Ion Transfer. *J. Mater. Chem. A* **2019**, *7* (14), 8633–8640.
- (15) Niyato, D.; Kim, D. I.; Maso, M.; Han, Z. Wireless Powered Communication Networks: Research Directions and Technological Approaches. *IEEE Wirel. Commun.* **2017**, *24* (6), 88–97.
- (16) Raj, A.; Steingart, D. Review—Power Sources for the Internet of Things. *J. Electrochem. Soc.* **2018**, *165* (8), B3130–B3136.
- (17) Luo, Y.; Pu, L.; Wang, G.; Zhao, Y. RF Energy Harvesting Wireless Communications: RF Environment, Device Hardware and Practical Issues. *Sensors* **2019**, *19* (13), 3010.
- (18) Malti, A.; Edberg, J.; Granberg, H.; Khan, Z. U.; Andreasen, J. W.; Liu, X.; Zhao, D.; Zhang, H.; Yao, Y.; Brill, J. W.; Engquist, I.; Fahlman, M.; Wågberg, L.; Crispin, X.; Berggren, M. An Organic Mixed Ion-Electron Conductor for Power Electronics. *Adv. Sci.* **2016**, *3* (2), 1500305.
- (19) Park, S.; Parida, K.; Lee, P. S. Deformable and Transparent Ionic and Electronic Conductors for Soft Energy Devices. *Adv. Energy Mater.* **2017**, *7* (22), 1701369.
- (20) Bryan, A. M.; Santino, L. M.; Lu, Y.; Acharya, S.; D'Arcy, J. M. Conducting Polymers for Pseudocapacitive Energy Storage. *Chem. Mater.* **2016**, *28* (17), 5989–5998.
- (21) Zhang, H.; Yao, M.; Wei, J.; Zhang, Y.; Zhang, S.; Gao, Y.; Li, J.; Lu, P.; Yang, B.; Ma, Y. Stable p/n-Dopable Conducting Redox Polymers for High-Voltage Pseudocapacitor Electrode Materials: Structure–Performance Relationship and Detailed Investigation into Charge-Trapping Effect. *Adv. Energy Mater.* **2017**, *7* (21), 1701063.
- (22) Wang, K.; Huang, L.; Eedugurala, N.; Zhang, S.; Sabuj, M. A.; Rai, N.; Gu, X.; Azoulay, J. D.; Ng, T. N. Wide Potential Window Supercapacitors Using Open-Shell Donor–Acceptor Conjugated Polymers with Stable N-Doped States. *Adv. Energy Mater.* **2019**, *9* (47), 1902806.
- (23) Österholm, A. M.; Ponder, J. F.; Kersulis, J. A.; Reynolds, J. R. Solution Processed PEDOT Analogues in Electrochemical Supercapacitors. *ACS Appl. Mater. Interfaces* **2016**, *8* (21), 13492–13498.
- (24) Lehtimäki, S.; Li, M.; Salomaa, J.; Pörhönen, J.; Kalanti, A.; Tuukkanen, S.; Heljo, P.; Halonen, K.; Lupo, D. Performance of Printable Supercapacitors in an RF Energy Harvesting Circuit. *Int. J. Electr. Power Energy Syst.* **2014**, *58*, 42–46.
- (25) Gaikwad, A. M.; Steingart, D. A.; Ng, T. N.; Schwartz, D. E.; Whiting, G. L. A Flexible High Potential Printed Battery for Powering Printed Electronics. *Appl. Phys. Lett.* **2013**, *102* (23), 233302.
- (26) Ng, T. N.; Schwartz, D. E.; Mei, P.; Kor, S.; Veres, J.; Bröms, P.; Karlsson, C. Pulsed Voltage Multiplier Based on Printed Organic Devices. *Flex. Print. Electron.* **2016**, *1* (1), 015002.
- (27) Manjakkal, L.; Pullanchiyodan, A.; Yogeswaran, N.; Hosseini, E. S.; Dahiya, R. A Wearable Supercapacitor Based on Conductive PEDOT:PSS-Coated Cloth and a Sweat Electrolyte. *Adv. Mater.* **2020**, *32* (24), 1907254.
- (28) Abo-Farha, S. A.; Abdel-Aal, A. Y.; Ashour, I. A.; Garamon, S. E. Removal of Some Heavy Metal Cations by Synthetic Resin Purolite C100. *J. Hazard. Mater.* **2009**, *169* (1), 190–194.
- (29) Ran, J.; Wu, L.; He, Y.; Yang, Z.; Wang, Y.; Jiang, C.; Ge, L.; Bakangura, E.; Xu, T. Ion Exchange Membranes: New Developments and Applications. *J. Membr. Sci.* **2017**, *522*, 267–291.
- (30) Silva, R. A.; Hawboldt, K.; Zhang, Y. Application of Resins with Functional Groups in the Separation of Metal Ions/Species – a Review. *Miner. Process. Extr. Metall. Rev.* **2018**, *39* (6), 395–413.
- (31) Li, Y.; Ren, G.; Zhang, Z.; Teng, C.; Wu, Y.; Lu, X.; Zhu, Y.; Jiang, L. A Strong and Highly Flexible Aramid Nanofibers/PEDOT: PSS Film for All-Solid-State Supercapacitors with Superior Cycling Stability. *J. Mater. Chem. A* **2016**, *4* (44), 17324–17332.
- (32) Niu, J.; Conway, B. E.; Pell, W. G. Comparative Studies of Self-Discharge by Potential Decay and Float-Current Measurements at C Double-Layer Capacitor and Battery Electrodes. *J. Power Sources* **2004**, *135* (1), 332–343.
- (33) Kowal, J.; Avaroglu, E.; Chamekh, F.; Šenfelds, A.; Thien, T.; Wijaya, D.; Sauer, D. U. Detailed Analysis of the Self-Discharge of Supercapacitors. *J. Power Sources* **2011**, *196* (1), 573–579.
- (34) Ricketts, B. W.; Ton-That, C. Self-Discharge of Carbon-Based Supercapacitors with Organic Electrolytes. *J. Power Sources* **2000**, *89* (1), 64–69.
- (35) Andreas, H. A.; Lussier, K.; Oickle, A. M. Effect of Fe-Contamination on Rate of Self-Discharge in Carbon-Based Aqueous Electrochemical Capacitors. *J. Power Sources* **2009**, *187* (1), 275–283.
- (36) Tehrani, P.; Kanciurzewska, A.; Crispin, X.; Robinson, N. D.; Fahlman, M.; Berggren, M. The Effect of PH on the Electrochemical Over-Oxidation in PEDOT:PSS Films. *Solid State Ionics* **2007**, *177* (39), 3521–3527.
- (37) Rinne, J.; Keskinen, J.; Berger, P. R.; Lupo, D.; Valkama, M. Viability Bounds of M2M Communication Using Energy-Harvesting and Passive Wake-Up Radio. *IEEE Access* **2017**, *5*, 27868–27878.
- (38) Yang, H.; Zhang, Y. Self-Discharge Analysis and Characterization of Supercapacitors for Environmentally Powered Wireless Sensor Network Applications. *J. Power Sources* **2011**, *196* (20), 8866–8873.
- (39) Keskinen, J.; Lehtimäki, S.; Dastpak, A.; Tuukkanen, S.; Flyktman, T.; Kraft, T.; Railanmaa, A.; Lupo, D. Architectural Modifications for Flexible Supercapacitor Performance Optimization. *Electron. Mater. Lett.* **2016**, *12* (6), 795–803.
- (40) Kim, N.; Kee, S.; Lee, S. H.; Lee, B. H.; Kahng, Y. H.; Jo, Y.-R. R.; Kim, B.-J. J.; Lee, K. Highly Conductive PEDOT:PSS Nanofibrils Induced by Solution-Processed Crystallization. *Adv. Mater.* **2014**, *26* (14), 2268–2272.